ChemPubSoc Europe

DOI: 10.1002/ejic.201800359

EurJIC European Journal of Inorganic Chemistry

Full Paper

Single-Molecule Magnets | *Very Important Paper* |

Single-Crystal to Single-Crystal Transformations and Magnetic Properties of a Series of "Butterfly" $Ni^{II}_2Ln^{III}_2$ Compounds: SMM Behavior of the Dysprosium(III) Analogue

Shuvankar Mandal,[a] Sagar Ghosh,[a] Daisuke Takahashi,[b] George Christou,*[b] and Sasankasekhar Mohanta*[a]

Abstract: This investigation reports syntheses, crystal structures, and magnetic properties of a series of "butterfly" $Ni^{II}_2Ln^{III}_2$ compounds of compositions $[Ni^{II}_2Ln^{III}_2L_4(NO_3)_2(MeOH)_2]$ (**1**, Ln = Gd; **2**, Ln = Tb; **3**, Ln = Dy; **4**, Ln = Ho; **5**, Ln = Er) and $[Ni^{II}_2Ln^{III}_2L_4(NO_3)_2(H_2O)_2]\cdot 2H_2O$ (**1A**, Ln = Gd; **2A**, Ln = Tb; **3A**, Ln = Dy; **4A**, Ln = Ho; **5A**, Ln = Er), where H_2L is the Schiff base ligand, obtained on [1+1] condensation of 3-ethoxysalicylaldehyde and 2-aminophenol. The five compounds **1A**–**5A** are formed as a result of single-crystal to single-crystal transformations (SC–SC) of the five compounds **1**–**5**. The dc and ac magnetic measurements carried out for the five stable compounds **1A**–**5A** reveal the following: (i) overall ferromagnetic interaction exists in all of the $Ni^{II}_2Ln^{III}_2$ compounds **1A**–**5A**; (ii) both $Ni^{II}\cdots Ni^{II}$ and $Ni^{II}\cdots Gd^{III}$ interactions in the Gd^{III} analogue **1A** are ferromagnetic, with J values of 1.83(0.08) cm^{-1} and 0.285(0.002) cm^{-1}, respectively; and (iii) only the Dy^{III} analogue **3A** exhibits single-molecule magnet (SMM) properties, with an energy barrier (U_{eff}) of 25 cm^{-1} and a relaxation time (τ_0) of 8×10^{-8} s. Comparison of the structures and properties of the compounds in the present investigation with those of analogous systems derived from a related ligand reveals remarkable differences.

Introduction

Slow relaxation of magnetization after the removal of the applied magnetic field was observed for the first time in a discrete molecule by Gatteschi and co-workers in the early 1990s; the concerned molecule, that is, the first single-molecule magnet (SMM), is a dodecanuclear $Mn^{III}_8Mn^{IV}_4$ cluster.[1] The major difference between conventional magnets or molecule-based extended magnets and SMMs is that the magnetic memory of SMMs arises solely from the molecule itself, whereas it is a bulk phenomenon in the former class. SMMs have potential applications in high-density data storage devices, quantum computing, spintronics devices, and magnetic refrigeration.[2] Therefore, this area has been a frontier research field during the last two–three decades. As the first SMM is a polynuclear cluster of mixed-valence manganese(III) and manganese(IV), a lot of effort has been directed towards clusters of 3d metal ions (e.g., $Mn^{III}/Mn^{II}/Mn^{IV}/Ni^{II}/Co^{II}/Fe^{III}$) in exploring the area of SMMs.[2–4] However, all of those SMMs exhibit slow relaxation only below 5 K and the maximum U_{eff} obtained is only 62 cm^{-1}.[3e] It was understood that large uniaxial anisotropy (i.e., a negative zero-field splitting parameter) and a large spin ground state are required for better SMMs [i.e., SMMs having greater energy barriers (U_{eff}) to magnetization reversal and greater blocking temperatures (T_B)]. Later, it was realized that lanthanides would be better members for SMMs, as most of the lanthanides are associated with large anisotropy. The study of lanthanides in the area of SMMs was started with the report of the slow relaxation of magnetization in $[NBu_4][Tb(phthalocyanine)_2]$ with U_{eff} = 230 cm^{-1}.[5] This breakthrough invention was followed by a flood of reports of 4f and also 3d–4f SMMs of various nuclearity (mono/di/oligo/polynuclear).[2a,2h,6–19] Recently, molecular magnetic hysteresis at 60 K, the maximum so far, has been observed in a mononuclear dysprosium(III) system.[7a] Clearly, exploration of the magnetic properties of lanthanide-containing compounds deserves attention.

The 3d–4f coordination cluster with butterfly topology is a familiar structural motif in magnetochemistry. In the last few years, a number of heterotetrametallic "butterfly" complexes of 3d and 4f metal ions have been reported. In terms of metal–metal combinations, these systems include: $Co^{III}_2Ln^{III}_2$ (Ln = Gd, Tb, Dy, Ho, Er, Yb);[11] $Cr^{III}_2Ln^{III}_2$ (Ln = Pr, Nd, Tb, Dy, Er, Ho);[11a,12] $Mn^{III}_2Ln^{III}_2$ (Ln = La, Ce, Pr, Nd, Eu, Gd, Tb, Dy, Er);[13] $Mn^{IV}_2Ln^{III}_2$ (Ln = Yb),[14a] $Fe^{III}_2Ln^{III}_2$ (Ln = Ce–Yb);[14] $Co^{II}_2Ln^{III}_2$ (Ln = Gd–Er);[13c,15] $Cu^{II}_2Ln^{III}_2$ (Ln = Gd–Er);[13c] and $Ni^{II}_2Ln^{III}_2$ (Ln = Gd–Er).[13c,16] The two lanthanide(III) ions occupy the "body" position in some of these complexes, but the "wing" position in

[a] *Department of Chemistry, University of Calcutta, 92 Acharya Prafulla Chandra Road, Kolkata 700009, India*
E-mail: sm_cu_chem@yahoo.co.in
http://www.caluniv.ac.in/academic/department/Chemistry/Sasankasekhar-Mohanta.pdf
[b] *Department of Chemistry, University of Florida, Gainesville, Florida 32611-7200, U. S. A.*
E-mail: christou@chem.ufl.edu
https://christou.chem.ufl.edu/
Supporting information and ORCID(s) from the author(s) for this article are available on the WWW under https://doi.org/10.1002/ejic.201800359.

others. All of the Dy^{III} analogues among these "butterflies" are SMMs. A few "butterflies" of other lanthanides (Tb^{III}, Ho^{III}, Er^{III}, Yb^{III}, Ce^{III}, Nd^{III}) are also known to show slow relaxation of magnetization.[11b,11c,12,13,14a,16a] Hence, the exploration of "butterfly" 3d–4f clusters deserves attention.

The family of Schiff base ligands, obtained on [1+1] condensation of 3-methoxysalicylaldehyde and an amino alcohol or an aminophenol, has occupied a dominant position in stabilizing 4f clusters[9] and 3d–4f clusters;[15–18] many examples have been reported in recent years and a number of them are SMMs. The beauty of such ligands to stabilize 3d–4f systems is that there are basically two types of pockets, one comprising phenoxo and alkoxido oxygen atoms and imine nitrogen atoms (pocket I; as in Scheme 1), which has the potential to bind with a 3d metal ion, and the second comprising phenoxo and ether (methoxy) oxygen atoms (pocket II; as in Scheme 1), which has the potential to bind with a 4f metal ion. Notably, although 3-ethoxysalicylaldehyde is very close to 3-methoxysalicylaldehyde, the former has been little utilized as a 3-ethoxysalicylaldehyde–amino alcohol/aminophenol ligand to isolate either 4f– or 3d–4f systems; during the progress of this work, only one paper dealing with three $M^{II}_2Dy^{III}_2$ (M = Zn, Co, Mn) compounds has been reported.[19] Based on our experience of drastic differences[20] in a number of cases among the metal complexes derived from 3-methoxysalicylaldehyde-diamine and 3-ethoxysalicylaldehyde-diamine ligands, we anticipated that structures and properties of the 3d–4f clusters in the 3-ethoxysalicylaldehyde–amino alcohol/aminophenol ligand environment may be different from those derived from 3-methoxysalicylaldehyde–amino alcohol/aminophenol ligand environment. Therefore, we felt it relevant to explore the structure and magnetic properties of 3d–4f compounds derived from 3-ethoxysalicylaldehyde–amino alcohol/aminophenol ligands. Accordingly, we report herein the syntheses, characterization, and crystal structures of a series of isomorphous ten "butterfly" $Ni^{II}_2Ln^{III}_2$ compounds of compositions $[Ni^{II}_2Ln^{III}_2L_4(NO_3)_2(MeOH)_2]$ (**1**, Ln = Gd; **2**, Ln = Tb; **3**, Ln = Dy; **4**, Ln = Ho; **5**, Ln = Er) and $[Ni^{II}_2Ln^{III}_2L_4(NO_3)_2(H_2O)_2]\cdot 2H_2O$ (**1A**, Ln = Gd; **2A**, Ln = Tb; **3A**, Ln = Dy; **4A**, Ln = Ho; **5A**, Ln = Er), along with the dc and ac magnetic properties of **1A**–**5A** (H_2L is the Schiff base ligand (Scheme 1), obtained on [1+1] condensation of 3-ethoxysalicylaldehyde and 2-aminophenol). Interestingly, single-crystal to single-crystal transformations take place in **1**–**5** to form **1A**–**5A**.

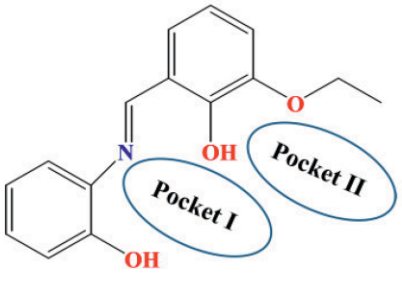

Scheme 1. Chemical structure of H_2L ligand, showing two types of pocket (I and II).

Result and Discussion

Syntheses and Characterization

The tetranuclear $Ni^{II}_2Ln^{III}_2$ compounds **1**–**5** were prepared in good yield, by following a similar procedure, where nickel(II) nitrate hexahydrate and the respective hydrated lanthanide(III) nitrate were treated with a methanol solution of H_2L in the presence of Et_3N (TEA) in a 1:1:2:4 stoichiometric ratio. When **1**–**5** were exposed to the open atmosphere, the compounds **1A**–**5A** were formed by single-crystal to single-crystal transformations, in which two coordinated methanol molecules are substituted by two water molecules and two other water molecules are incorporated as the solvent of crystallization (vide infra). The transformation of **1**–**5** to **1A**–**5A** is not associated with any visual change in color or any visual change in shininess. However, the FTIR spectra indicate that **1**–**5** are stable for a maximum period of around 20 minutes, because the spectra of **1**–**5** recorded one day or few days after their isolation are superimposable on those recorded 20 minutes after their isolation, but are different from those recorded immediately after their isolation.

The FTIR spectra of the ten compounds **1**–**5** and **1A**–**5A** are shown in Figures S1–S5. The characteristic C=N stretching in **1**–**5** and **1A**–**5A** appears as a strong band, almost at the same position (1604–1606 cm^{-1}). The appearance of two signals with very strong intensities at 1385–1388 cm^{-1} and 1292 cm^{-1} for **1**–**5** and at 1385–1388 cm^{-1} and 1293–1298 cm^{-1} for **1A**–**5A** indicates the presence of nitrate groups. Although most of the FTIR spectroscopic signals of **1**–**5** are practically identical to those of **1A**–**5A**, the spectra of the two sets of compounds are clearly different with respect to the two signals, as follows: (i) for **1**–**5**, medium-intensity signals, which can be assigned to the coordinated methanol molecules, appear at 3356–3358 cm^{-1}, whereas for **1A**–**5A**, a wider medium-intensity bands, which can be assigned to the coordinated and solvated water molecules, appear at 3418–3427 cm^{-1}; (ii) the medium-intensity peaks at 1519 cm^{-1} in the spectra for **1**–**5** are shifted to weak-intensity shoulders at 1512 cm^{-1} in the spectra for **1A**–**5A**. The similarity in most of the vibrations reveals the similarity in the tetranuclear cores (except for coordinated methanol versus coordinated water; vide infra), while the clear difference in the two signals reveals that the two sets of compounds are different and this difference in the FTIR spectra arises due to single-crystal to single-crystal transformations, which are described below; that is, the solid-state transformation, in this case, can be clearly seen with FTIR spectroscopy.

Description of the Crystal Structures of the $Ni^{II}_2Ln^{III}_2$ Compounds 1A–5A

The five $Ni^{II}_2Ln^{III}_2$ compounds **1A**–**5A** crystallize in the same space group $P\bar{1}$ with practically identical unit-cell parameters (Table 1). So, **1A**–**5A** are isomorphous. Their internal structures are also similar. The structure of one compound, **1A** (the Gd^{III} analogue), is described below in detail, followed by a comparison of the structural parameters of all of the five compounds.

Table 1. Crystallographic data for **1A**–**5A**.

	1A (Ni_2Gd_2)	**2A** (Ni_2Tb_2)	**3A** (Ni_2Dy_2)	**4A** (Ni_2Ho_2)	**5A** (Ni_2Er_2)
Formula	$C_{60}H_{56}N_6O_{22}Ni_2Gd_2$	$C_{60}H_{56}N_6O_{22}Ni_2Tb_2$	$C_{60}H_{56}N_6O_{22}Ni_2Dy_2$	$C_{60}H_{56}N_6O_{22}Ni_2Ho_2$	$C_{60}H_{56}N_6O_{22}Ni_2Er_2$
Formula mass [g/mol]	1645.02	1648.36	1655.52	1660.38	1665.04
Crystal system	triclinic	triclinic	triclinic	triclinic	triclinic
Space group	$P\bar{1}$	$P\bar{1}$	$P\bar{1}$	$P\bar{1}$	$P\bar{1}$
a [Å]	11.216(6)	11.2256(8)	11.244(3)	11.1903(7)	11.1893(8)
b [Å]	11.685(6)	11.7220(8)	11.700(4)	11.6606(8)	11.6383(8)
c [Å]	13.370(7)	13.4123(10)	13.439(4)	13.3897(9)	13.3907(9)
α [°]	79.369(7)	79.592(2)	79.269(4)	79.562(2)	79.392(2)
β [°]	65.441(6)	65.537(2)	65.423(3)	65.544(2)	65.489(2)
γ [°]	69.522(6)	69.545(2)	69.331(4)	69.452(2)	69.254(2)
V [Å^3]	1491.6(14)	1503.81(19)	1502.7(8)	1487.90(17)	1482.36(18)
Z	1	1	1	1	1
Temperature [K]	296(2)	296(2)	296(2)	296(2)	296(2)
2θ	3.35–49.7	3.34–51.2	3.34–49.89	3.34–51.4	3.35–51.7
μ [mm^{-1}]	2.903	3.025	3.161	3.340	3.515
$D_{calcd.}$ [g cm^{-3}]	1.831	1.820	1.829	1.853	1.865
F(000)	818	820	822	824	826
Absorption correction	multiscan	multiscan	multiscan	multiscan	multiscan
Index ranges	$-13 \le h \le 12$	$-13 \le h \le 13$	$-13 \le h \le 13$	$-13 \le h \le 13$	$-13 \le h \le 13$
	$-12 \le k \le 13$	$-14 \le k \le 14$	$-13 \le k \le 13$	$-14 \le k \le 14$	$-14 \le k \le 14$
	$-15 \le l \le 15$	$-14 \le l \le 16$	$-15 \le l \le 15$	$-16 \le l \le 15$	$-15 \le l \le 16$
Reflections collected	10174	17491	10358	17791	17609
Independent reflections (R_{int})	5068 (0.0394)	5546 (0.0421)	5162 (0.0427)	5552 (0.0398)	5626 (0.0513)
R_1[a]/wR_2[b] [$I > 2\sigma(I)$]	0.0408/0.0877	0.0364/0.0800	0.0404/0.0770	0.0333/0.0735	0.0409/0.0800
R_1[a]/ wR_2[b] [for all F_o^2]	0.0619/0.0972	0.0490/0.0865	0.0584/0.0840	0.0413/0.0774	0.0575/0.0866

[a] $R_1 = [\Sigma||F_o| - |F_c||/\Sigma|F_o|]$. [b] $wR_2 = [\Sigma w(F_o^2 - F_c^2)^2/\Sigma w(F_o^2)^2]^{1/2}$.

The crystal structure of the $Ni^{II}_2Gd^{III}_2$ compound **1A** is shown in Figure 1, while a simplified schematic of its structure is shown in Scheme 2. The selected bond lengths and angles in **1A** are listed in Table 2. One half of the structure is symmetry-related to the other half. The structure contains four deprotonated Schiff base ligands, $[L]^{2-}$, where both of the phenoxo moieties of H_2L are deprotonated. In terms of the atom labels of O(phenoxo)N(imine)O(phenoxo)O(ethoxy), the four ligand moieties are O2N1O1O3 (Ligand **1**; pocket I – O2N1O1; pocket II – O1O3), O5AN2O4O6 (Ligand **2**; pocket I – O5AN2O4; pocket II – O4O6), O2AN1AO1AO3A (Ligand **1A**; pocket I – O2AN1AO1A; pocket II – O1AO3A), and O5N2AO4AO6A (Ligand **2A**; pocket I – O5N2AO4A; pocket II – O4AO6A). Clearly, Ligand **1** and Ligand **1A** are symmetry-related, as are Ligand **2** and Ligand **2A**, two nickel(II) ions (Ni1 and Ni1A), and two gadolinium(III) ions (Gd1 and Gd1A). Gd1 is chelated by both pocket I (O2N1O1) of Ligand **1** and pocket II (O4O6) of Ligand **2**, while Ni1 is chelated by pocket I (O5AN2O4) of Ligand **2**. Clearly, both of the pockets of Ligand **2** are occupied by metal ions (Ni1 in one and Gd1 in the second). On the other hand, although the phenoxo oxygen atom (O1) of pocket II of Ligand **1** is coordinated to Gd1, the ethoxy oxygen atom (O3) of this pocket is non-coordinated; that is, pocket II of Ligand **1** is vacant. Interlinking of the Ni1Gd1–Ligand **1**–Ligand **2** and Ni1AGd1A–Ligand **1A**–Ligand **2A** fragments takes place through the four phenoxo oxygen

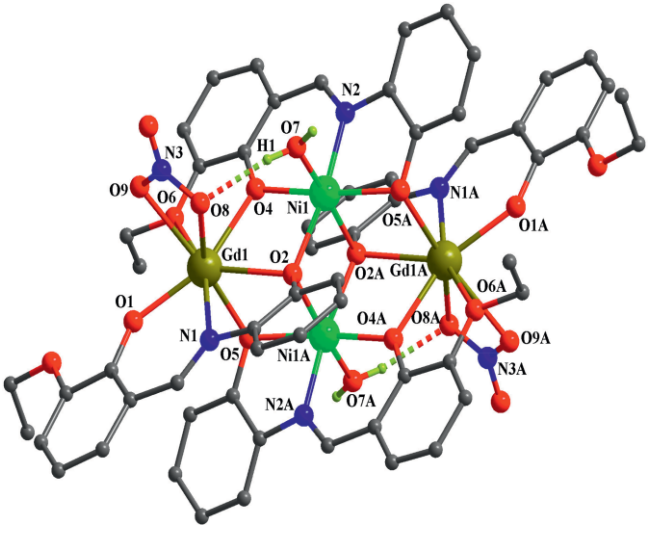

Figure 1. Crystal structure of $[Ni^{II}_2Gd^{III}_2L_4(NO_3)_2(H_2O)_2]\cdot 2H_2O$ (**1A**). Solvated water molecules and hydrogen atoms, except those of coordinated water molecules, are omitted for clarity. Symmetry code: A, 1 – *x*, 2 – *y*, 1 – *z*.

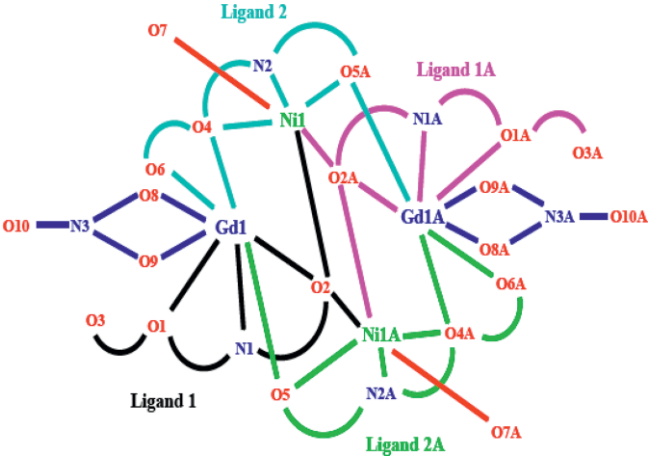

Scheme 2. Simplified schematic presentation of **1A**.

Table 2. Selected bond lengths [Å] and bond angles [°] in the coordination environment in **1A**–**5A**.

	1A (Ln = Gd)	**2A** (Ln = Tb)	**3A** (Ln = Dy)	**4A** (Ln = Ho)	**5A** (Ln = Er)
Bond lengths					
Ni1–N2	1.990(5)	1.997(4)	1.991(5)	1.991(3)	1.992(4)
Ni1–O2	2.094(4)	2.095(3)	2.094(4)	2.088(3)	2.088(3)
Ni1–O2A	2.136(4)	2.141(3)	2.137(4)	2.139(3)	2.139(3)
Ni1–O4	2.002(4)	2.013(3)	2.012(4)	2.005(3)	1.993(3)
Ni1–O5A/O5	2.053(4)	2.058(3)	2.066(4)	2.059(3)	2.059(3)
Ni1–O7	2.111(6)	2.128(4)	2.136(6)	2.129(4)	2.124(5)
Ln1–N1	2.462(5)	2.453(4)	2.450(5)	2.426(4)	2.416(4)
Ln1–O1	2.170(4)	2.164(3)	2.144(4)	2.145(3)	2.137(4)
Ln1–O2	2.412(4)	2.414(3)	2.400(3)	2.386(3)	2.375(3)
Ln1–O4	2.303(4)	2.301(3)	2.284(4)	2.271(3)	2.261(3)
Ln1–O5/O5A	2.308(4)	2.304(3)	2.287(4)	2.270(3)	2.259(4)
Ln1–O6	2.516(4)	2.517(3)	2.509(4)	2.493(3)	2.490(4)
Ln1–O8	2.471(5)	2.478(4)	2.455(5)	2.448(3)	2.435(4)
Ln1–O9	2.497(5)	2.493(4)	2.473(5)	2.460(4)	2.448(4)
Ni1···Ni1A	3.214	3.224	3.216	3.206	3.200
Ni1···Ln1	3.4721(14)	3.4765(6)	3.4715(10)	3.4562(6)	3.4471(7)
Ni1A···Ln1	3.4247(16)	3.4240(6)	3.4192(11)	3.3995(6)	3.3905(7)
O2–Ni1Ln1Ni1A	1.055	1.054	1.049	1.051	1.052
Bridge angles					
Ni1–O2–Ni1A	98.89(16)	99.16(12)	98.95(15)	98.65(11)	98.41(13)
Ni1–O2–Ln1	100.56(14)	100.65(12)	100.94(14)	100.95(11)	100.95(13)
Ni1–O4–Ln1	107.30(15)	107.20(13)	107.65(16)	107.67(12)	108.07(16)
Ni1A–O2–Ln1	97.50(14)	97.29(11)	97.62(14)	97.24(10)	97.26(13)
Ni1A–O5/O5A–Ln1	103.31(16)	103.30(13)	103.39(17)	103.40(12)	103.37(15)
Cisoid angle ranges (Ni^{II}–center)	81.11(16)–105.74(15)	80.84(12)–105.93(12)	81.05(15)–106.15(15)	81.09(11)–106.25(11)	80.79(14)–106.41(14)
Transoid angle ranges (Ni^{II}–center)	169.00(18)–172.01(17)	169.33(15)–171.97(14)	169.40(18)–171.77(17)	169.44(14)–171.65(13)	169.68(17)–171.60(16)
X–Ln1–Y (X, Y = N or O)	51.17(16)–160.29(14)	51.14(13)–159.85(12)	51.54(16)–159.33(14)	51.81(12)–159.04(11)	51.66(15)–158.93(14)

atoms, O2, O2A, O5, and O5A; O2/O2A acts as a μ_3-donor center (μ_3-phenoxo) and is coordinated to three metal ions, Ni1, Ni1A, and Gd1/Gd1A, while O5A/O5 acts as a μ-donor center (μ-phenoxo) and is coordinated to one Ni^{II} (Ni1/Ni1A) and one Gd^{III} (Gd1A/Gd1) ion. The gadolinium(III) center is also chelated by two oxygen atoms of a nitrate ligand and the nickel(II) center is coordinated by a water molecule. There are two waters of crystallization, as well.

The bridging pattern in **1A** may be summarized as follows: (i) the two metal ions in each of the four Ni^{II}···Gd^{III} pairs are bridged by one μ-phenoxo and one μ_3-phenoxo oxygen atom, where the four Ni^{II}-μ_3-phenoxo–Gd^{III} bridge angles (97.50°, 100.56°) are smaller than the four Ni^{II}–μ-phenoxo–Gd^{III} bridge angles (107.3°, 103.31°); (ii) the two nickel(II) centers are bridged by two μ_3-phenoxo oxygen atoms, where the two Ni^{II}–μ_3-phenoxo–Ni^{II} bridge angles are 98.89°; and (iii) there is no direct bridge between the two gadolinium(III) centers.

The central $[Ni^{II}_2Gd^{III}_2(\mu_3\text{-}O)_2]$ moiety in **1A** has a "butterfly" topology, in which two Ni^{II} ions are on the "body" position and two Gd^{III} ions are on the "wing" position of the butterfly; the four metal ions define a perfect plane and the two μ_3-phenoxo oxygen atoms are displaced above the tetrametallic plane by 1.055 Å.

The nickel(II) center is hexacoordinate with two μ-phenoxo, two μ_3-phenoxo, and one water oxygen atom, as well as one imine nitrogen atom. The $NiNO_5$ coordination environment is distorted octahedral, in which the ranges of the bond lengths and *cisoid* and *transoid* angles are, respectively, 1.990–2.136 Å, 81.11–105.74°, and 169.00–172.01°. The order of the bond lengths involving Ni^{II} is Ni^{II}–imine (Ni1–N2 = 1.990 Å) < Ni^{II}–μ-phenoxo (that bridges two metal ions in the two pockets of the same ligand; Ni1–O4 = 2.002 Å) < Ni^{II}–μ-phenoxo (that bridges two metal ions in the two pockets of the different ligands; Ni1–O5A = 2.053 Å) < Ni^{II}–μ_3-phenoxo (one of the two μ_3-phenoxo moieties; Ni1–O2 = 2.094 Å) < Ni^{II}–water (Ni1–O7 = 2.111 Å) < Ni^{II}–μ_3-phenoxo (second μ_3-phenoxo moiety; Ni1–O2A = 2.136 Å).

The gadolinium(III) center is octacoordinate with two μ-phenoxo, one μ_3-phenoxo, one monodentate phenoxo, one ethoxy, and two chelating nitrate oxygen atoms, as well as one imine nitrogen atom. A SHAPE[21] analysis (Table 3) reveals that triangular dodecahedron (TDD) is the "most ideal" geometry, although the deviations from the corresponding ideal geometry are close for all of the four possible cases: triangular dodecahedron (TDD, deviation = 2.56); biaugmented trigonal prism (BTPR, deviation = 2.76); biaugmented trigonal prism J50 (JBTPR, deviation = 3.08); and square antiprism (SAPR, deviation = 3.36). The range of the bond angles involving Gd in the $GdNO_7$ coordination environment is 51.17–160.29°. The order of the bond lengths involving Gd^{III} is Gd^{III}–monodentate phenoxo (Gd1–O1 = 2.170 Å) < Gd^{III}–μ-phenoxo (Gd1–O4 = 2.303 Å, Gd1–O5 = 2.308 Å) < Gd^{III}–μ_3-phenoxo (Gd1–O2 = 2.412 Å) < Gd^{III}–imine (Gd1–N1 = 2.462 Å) < Gd^{III}–nitrate (Gd1–O8 = 2.471 Å, Gd1–O9 = 2.497 Å) < Gd^{III}–ethoxy (Gd1–O6 = 2.516 Å).

There are two intramolecular hydrogen bonds per tetranuclear cluster, with each (O7–H1···O8/O7A–H1A···O8A) involving

Table 3. Continuous shape measures calculation for **1**–**5**, **1A**–**5A**, **8**, and **9** obtained using SHAPE.[21]

Compounds	TDD[a]	BTPR[a]	JBTPR[a]	SAPR[a]
1	2.637	2.671	2.992	3.318
2	2.589	2.672	2.947	3.304
3	572	2.627	2.915	3.246
4	2.519	2.555	2.832	3.154
5	2.464	2.481	2.755	3.100
1A	2.564	2.760	3.083	3.362
2A	2.524	2.740	3.035	3.305
3A	2.494	2.712	2.980	3.305
4A	2.444	2.628	2.906	3.220
5A	2.449	2.639	2.898	3.242
8[b]	3.236	3.763	3.926	4.091
9[b]	2.640	2.859	3.177	3.492

[a] TDD = Triangular dodecahedron; BTPR = Biaugmented trigonal prism; JBTPR = Biaugmented trigonal prism J50; SAPR = Square antiprism. [b] Published in ref.[16a]; SHAPE analyses are done in this report.

one water hydrogen atom and one coordinated oxygen atom of the nitrate ligand.

As already mentioned, the five compounds **1A**–**5A** are isomorphous and isostructural. The crystal structure of the Dy^{III} analogue (**3A**) is shown in Figure 2, while those of the other three compounds are shown in Figures S6–S8. The selected bond lengths and angles in **1A**–**5A** are compared in Table 2, and the results of the SHAPE analysis are listed in Table 3. As expected from lanthanide contraction, a gradual decrease in the bond lengths should occur on going from Gd^{III} to Er^{III}. However, although the decrease is not systematic for all of the neighboring pairs, an overall decrease takes place in all eight types of bonds: The values of overall decrease for the Ln^{III}–monodentate phenoxo (Ln1–O1), Ln^{III}–μ-phenoxo (Ln1–O4/Ln1–O5/O5A), Ln^{III}–μ_3-phenoxo (Ln1–O2), Ln^{III}–imine (Ln1–N1), Ln^{III}–nitrate (Ln1–O8/Ln1–O9), and Ln^{III}–ethoxy (Ln1–O6) bond lengths are 0.033, 0.042/0.049, 0.037, 0.046, 0.036/0.049, and 0.026 Å, respectively. The order of the bond lengths involving Gd^{III} in **1A** has been already discussed. Notably, the same order is valid for the bond lengths involving Ln^{III} in **2A**–**5A**: Ln^{III}–monodentate phenoxo (Ln1–O1) < Ln^{III}–μ-phenoxo (Ln1–O4, Ln1–O5/O5A) < Ln^{III}–μ_3-phenoxo (Ln1–O2) < Ln^{III}–imine (Ln1–N1) < Ln^{III}–nitrate (Ln1–O8, Ln1–O9) < Ln^{III}–ethoxy (Ln1–O6). The individual bond angles, and evidently the range of the bond angles in the coordination environment of the Ln^{III} centers in **1A**–**5A**, are practically identical.

The values of the structural parameters involving Ni^{II} centers in **1A**–**5A** are very close; the ranges of the differences in the corresponding Ni^{II}–N/O bond lengths and N/O–Ni^{II}–N/O angles in **1A**–**5A** are, respectively, 0.005–0.025 Å and 0.17–1.21°.

The ranges of the Ni–μ_3-phenoxo–Ni, two types of Ni–μ_3-phenoxo–Ln, and two types of Ni–μ-phenoxo–Ln bridge angles in **1A**–**5A** are 98.41–99.16°, 97.24–97.62°, 100.56–100.95°, 103.30–103.40°, and 107.20–108.07°, respectively: that is, the corresponding phenoxo bridge angles vary in the short range (the range of difference is 0.10–0.87°).

The geometries of the intramolecular hydrogen bond in **1A**–**5A** are listed in Table S1, revealing that the hydrogen bonds are moderately strong.

Description of the Crystal Structures of the $Ni^{II}_2Ln^{III}_2$ Compounds 1–5

The five $Ni^{II}_2Ln^{III}_2$ compounds **1**–**5** crystallize in the same space group, $P\bar{1}$, with practically identical unit-cell parameters (Table S2). The space group for **1**–**5** and **1A**–**5A** are the same, $P\bar{1}$, and the values of the unit-cell parameters for these ten compounds are also close. Hence, all of the ten compounds, **1**–**5** and **1A**–**5A**, are isomorphous. The crystal structure of the $Ni^{II}_2Er^{III}_2$ compound **5** is shown in Figure 3, while those of the other four compounds are shown in Figures S9–S12. Their internal structures are similar to each other and also to those of the already discussed $Ni^{II}_2Ln^{III}_2$ series **1A**–**5A**, except that: (i) an equivalent coordination position of each of the two symmetry-related

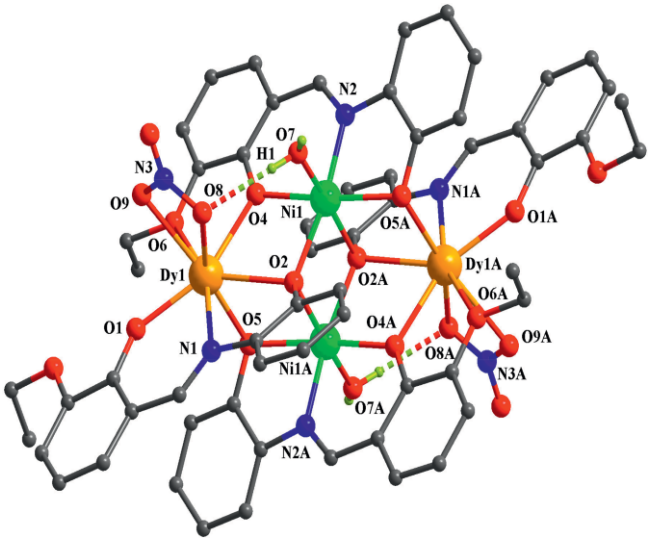

Figure 2. Crystal structure of $[Ni^{II}_2Dy^{III}_2L_4(NO_3)_2(H_2O)_2]\cdot 2H_2O$ (**3A**). Solvated water molecules and hydrogen atoms, except those of coordinated water molecules, are omitted for clarity. Symmetry code: A, 1 – *x*, 2 – *y*, 1 – *z*.

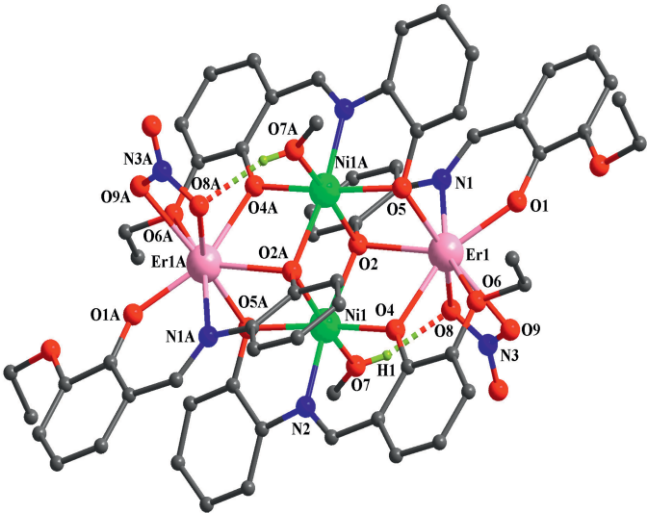

Figure 3. Crystal structure of $[Ni^{II}_2Er^{III}_2L_4(NO_3)_2(MeOH)_2]$ (**5**). Hydrogen atoms, except those of the O–H groups of the coordinated methanol molecules, are omitted for clarity. Symmetry code: A, –*x*, 1 – *y*, 1 – *z*.

nickel(II) centers in **1A**–**5A** and **1**–**5** is occupied by, respectively, a water molecule and a methanol molecule; and (ii) there is no solvent of crystallization in **1**–**5**, while **1A**–**5A** each contain two water molecules of crystallization.

As in **1A**–**5A**, there are two intramolecular hydrogen bonds in **1**–**5** per tetranuclear cluster, with each (O7–H1···O8/O7A–H1A···O8A) involving a methanol O–H hydrogen atom and one coordinated oxygen atom of the nitrate ligand. The geometries of the intramolecular hydrogen bonds in **1**–**5** are also listed in Table S1, revealing that these hydrogen bonds are also moderately strong.

The selected structural parameters in **1**–**5** are compared in Table S3. Bond angles in the coordination environment of the metal ions of the two $Ni^{II}Ln^{III}$ compounds, having the same lanthanide element in **1** and **1A**, **2** and **2A**, **3** and **3A**, **4** and **4A**, and **5** and **5A**, are compared in Tables S4–S13. Considering all five pairs, the differences in the corresponding bond lengths and bond angles in each pair of compounds in the coordination environment of the metal ions lie in the ranges 0.000–0.025 Å and 0.000–1.760°, respectively. The Ni–O/N and Ln–O/N bond lengths in **1**–**5** follow the same order as in **1A**–**5A**. Again, the geometry of Ni^{II} is similarly distorted octahedral and the geometry of Ln^{III} is similarly TDD (Table 3) in all of the ten compounds. Hence, except for the presence of two coordinated water molecules in each of **1A**–**5A** and two coordinated methanol molecules in each of **1**–**5** in equivalent positions, the tetrametallic cores in the two $Ni^{II}_2Ln^{III}_2$ compounds (having the same lanthanide element; one from **1**–**5** and the second from **1A**–**5A**, respectively) are practically identical.

Single-Crystal to Single-Crystal Transformations

As already mentioned, the five compounds of composition $[Ni^{II}_2Ln^{III}_2(L)_4(NO_3)_2(H_2O)_2]\cdot 2H_2O$ (**1A**–**5A**, Ln = Gd–Er) are produced on exposing the five compounds of composition $[Ni^{II}_2Ln^{III}_2(L)_4(NO_3)_2(MeOH)_2]$ (**1**–**5**, Ln = Gd–Er) to the open atmosphere. It has already been mentioned that compounds **1A**–**5A** are shiny and diffractable, from which their crystal structures have been determined. Clearly, this is a case of a single-crystal to single-crystal (SC–SC) transformation, in which two coordinated methanol molecules (coordinated to the two Ni^{II} centers) are substituted by two coordinated water molecules (coordinated to the two Ni^{II} centers) and two other water molecules are incorporated as the solvent of crystallization.

Previously, several types of SC–SC transformations have been reported. In most of the SC–SC transformations in metal complexes, the phenomenon is related to a change in the outside of the coordination sphere of the metal ions; these are of types that include the following: (i) removal of the solvent of crystallization;[22] (ii) exchange of the solvent of crystallization/guest species;[23] and (iii) chemical change.[24] On the other hand, although there are examples of the change of coordination sphere of the metal ions due to SC–SC transformations, the number is much less.[25,26] Again, most systems of the latter type are associated with either removal or addition of coordinated solvent molecules; there are only a few examples where exchange of coordinated solvent molecules takes place.[26] Clearly, the SC–SC transformation in this report is among the few cases where exchange of coordinated solvent molecules takes place.

Magnetic Properties

Variable-temperature magnetic susceptibilities of powdered samples of **1A**–**5A** were measured in the temperature range 5–300 K at an applied dc field of 0.1 T. The $\chi_M T$ versus T profiles of these five compounds are shown in Figure 4 (for the Gd^{III} analogue **1A**), Figure 5 (for the Tb^{III} analogue **2A**, Dy^{III} analogue **3A**, and Ho^{III} analogue **4A**) and Figure 6 (for the Er^{III} analogue **5A**). The $\chi_M T$ values at 300 K for **1A**–**5A** are, respectively, 19.07, 25.48, 28.37, 29.60, and 26.46 $cm^3\ K\ mol^{-1}$, which are close to the theoretical values (17.77, 25.64, 30.27, 30.12, and 24.89 $cm^3\ K\ mol^{-1}$, respectively) of two noninteracting Ni^{II} ions and two noninteracting Ln^{III} ions. The $\chi_M T$ versus T profiles of these five compounds are of three types: (i) Type 1 (for the Gd^{III}

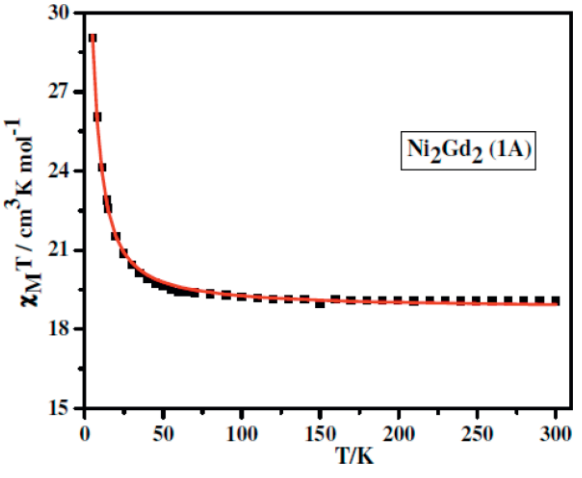

Figure 4. Plot of the $\chi_M T$ versus T of $[Ni^{II}_2Gd^{III}_2L_4(NO_3)_2(H_2O)_2]\cdot 2H_2O$ (**1A**) between 5 and 300 K under an applied dc magnetic field of 0.1 T. Symbols: experimental data. Solid lines: simulated data.

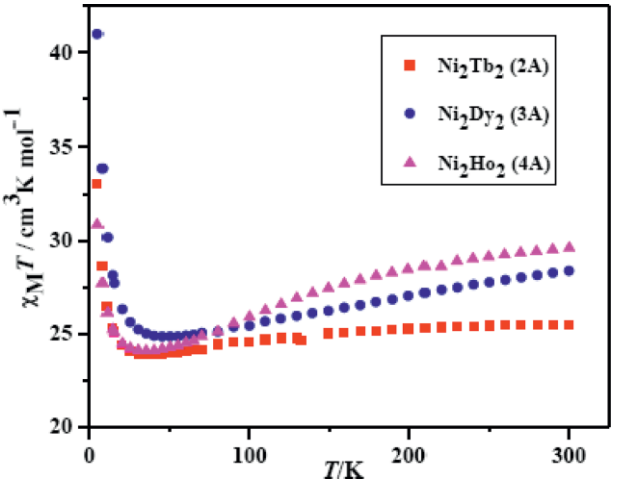

Figure 5. Plot of the $\chi_M T$ versus T of $[Ni^{II}_2Ln^{III}_2L_4(NO_3)_2(H_2O)_2]\cdot 2H_2O$ (**2A**, Ln = Tb; **3A**, Ln = Dy; **4A**, Ln = Ho) between 5 and 300 K under an applied dc magnetic field of 0.1 T.

analogue **1A**) – on lowering the temperature, the $\chi_M T$ value increases slowly to 20.13 cm^3 K mol^{-1} at 35 K and then sharply to 29.05 cm^3 K mol^{-1} at 5 K; (ii) Type 2 (for the Tb^{III}, Dy^{III}, and Ho^{III} analogues **2A**, **3A**, and **4A**) – with decreasing temperature, the $\chi_M T$ values decrease slowly to reach a minimum value of 23.85 cm^3 K mol^{-1} at 35 K for **2A**, 24.84 cm^3 K mol^{-1} at 50 K for **3A**, and 24.07 cm^3 K mol^{-1} at 35 K for **4A**, and then increase rapidly to 33.03 cm^3 K mol^{-1} for **2A**, 41.00 cm^3 K mol^{-1} for **3A**, and 30.85 cm^3 K mol^{-1} for **4A** at 5 K; and (iii) Type 3 (for the Er^{III} analogue **5A**) – on lowering the temperature, the $\chi_M T$ value decreases slowly to 25.79 cm^3 K mol^{-1} at 138 K and sharply to 21.67 cm^3 K mol^{-1} at 5 K. The profile of the Gd^{III} analogue indicates that the overall exchange interaction in this molecule is ferromagnetic throughout the temperature range, while the cryomagnetic behavior of the Tb^{III}, Dy^{III}, and Ho^{III} analogues reveals that the overall ferromagnetic interaction exists in these compounds only at low temperatures, where $\chi_M T$ increases on lowering the temperature. The overall intramolecular exchange interaction at low temperatures in the Er^{III} compound should be taken as very weakly ferromagnetic, as evidenced from the appearance of a plateau at the lowest temperatures in the dc $\chi_M T$ versus T plot (Figure 6), as well as from a slight increase in the ac in-phase $\chi_M' T$ data (in the Supporting Information) at the lowest temperatures. However, although overall ferromagnetic interaction is operative at low temperatures in the Tb^{III}, Dy^{III}, Ho^{III}, and Er^{III} analogues, no conclusion can be drawn regarding the nature of the $Ni^{II}\cdots Ln^{III}$ interactions, because the dominant interaction at low temperatures should be ferromagnetic, due to the stronger ferromagnetic $Ni^{II}\cdots Ni^{II}$ interaction [vide infra; 1.83(0.08) cm^{-1} in **1A**; should be similar in others], even if the $Ni^{II}\cdots Ln^{III}$ interaction is antiferromagnetic. However, as the $Ni^{II}\cdots Ni^{II}$ interaction is expectedly ferromagnetic in **2A**/**3A**/**4A**/**5A** and as the $Ni^{II}\cdots Ln^{III}$ interaction can be perceivable at low temperatures only (deep-seated 4f orbitals), the decrease in $\chi_M T$ at higher temperatures on lowering the temperatures in these four compounds of anisotropic lanthanides can be reasonably rationalized in terms of the depopulation of the upper Stark sublevels.

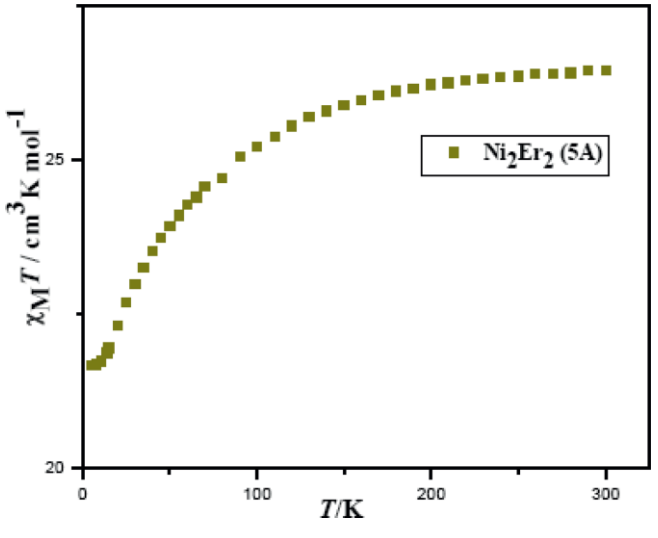

Figure 6. Plot of the $\chi_M T$ versus T of $[Ni^{II}_2Er^{II}_2L_4(NO_3)_2(H_2O)_2]\cdot 2H_2O$ (**5A**) between 5 and 300 K under an applied dc magnetic field of 0.1 T.

The magnetization (M) data up to 5 T at 2.5 and 5 K for **1A** and at 2.5, 5, and 10 K for **2A**–**5A** have been collected, and they are shown in Figure 7 for **1A** (Gd^{III}) and Figures S13–S16 for **2A**–**5A**, respectively. The M versus H/T plots (Figure 8 for **3A**, Figures S17–S20 for **1A**, **2A**, **4A**, and **5A**), reveal that the plots of all five compounds do not pass through a master curve and that such deviation is prominent for the Tb^{III}–Er^{III} analogues, indicates anisotropy or low-lying excited states in these systems.

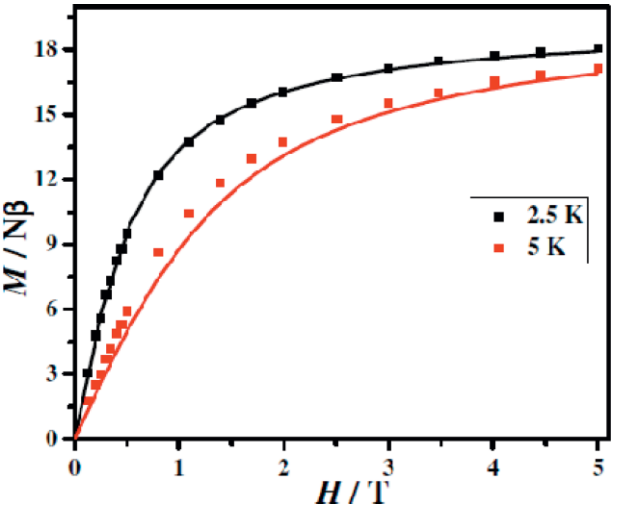

Figure 7. Magnetization (M versus H) $[Ni^{II}_2Gd^{III}_2L_4(NO_3)_2(H_2O)_2]\cdot 2H_2O$ (**1A**) at the indicated temperatures. The symbols are the experimental data, while the solid lines represent the fitted curves.

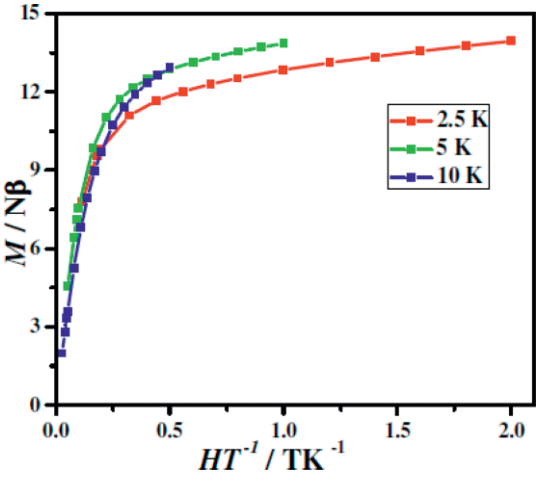

Figure 8. Plot M versus H/T of $[Ni^{II}_2Dy^{III}_2L_4(NO_3)_2(H_2O)_2]\cdot 2H_2O$ (**3A**) at the indicated temperatures.

In principle, the magnetic exchange interactions for the Ni1···Gd1/Ni1A···Gd1A should be different from Ni1···Gd1A/Ni1A···Gd1. However, as the $Ni^{II}\cdots Gd^{III}$ interactions should be small, it is logical that all of the $Ni^{II}\cdots Gd^{III}$ interactions are the same. Then, the magnetic properties of **1A** can be modeled by the following Hamiltonian (according to Scheme 3):

$\hat{\mathbf{H}} = -2J_1(\hat{\mathbf{S}}_1 \cdot \hat{\mathbf{S}}_3) - 2J_2(\hat{\mathbf{S}}_1 \cdot \hat{\mathbf{S}}_2 + \hat{\mathbf{S}}_1 \cdot \hat{\mathbf{S}}_4 + \hat{\mathbf{S}}_2 \cdot \hat{\mathbf{S}}_3 + \hat{\mathbf{S}}_3 \cdot \hat{\mathbf{S}}_4)$

where $\hat{\mathbf{S}}_1 = \hat{\mathbf{S}}_3 = 1$ and $\hat{\mathbf{S}}_2 = \hat{\mathbf{S}}_4 = 7/2$. With this model and using the PHI software,[27] both $\chi_M T$ versus T and M versus H data can

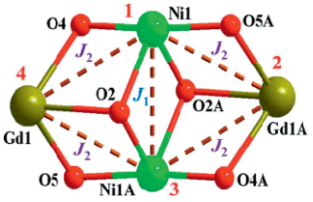

Scheme 3. Model of magnetic exchange for **1A**.

only be contemporaneously simulated on taking into account the single-ion zero-field effect of Ni^{II}. The obtained converging parameters are J_1 = 1.83(0.08) cm^{-1}, J_2 = 0.285(0.002) cm^{-1}, D_{Ni} = 8.35(0.21) cm^{-1}, g_{Ni} = 2.228(0.008), and g_{Gd} = 2.034(0.001).

Variable-temperature (1.8–15 K) ac susceptibilities of the five compounds **1A**–**5A** were measured under zero dc field and at one or more frequencies. The in-phase and out-of-phase susceptibilities of the Gd^{III} (**1A**), Tb^{III} (**2A**), Ho^{III} (**4A**), and Er^{III} (**5A**) analogues are shown in Figures S21–S24, while those of the Dy^{III} (**3A**) analogue are shown in Figures 9 and 10. There is no detectable out-of-phase susceptibility at a sufficiently higher frequency (997 Hz) for the Gd^{III}, Tb^{III}, Ho^{III}, and Er^{III} analogues. The out-of-phase data for the Tb^{III} analogue is practically non-detectable at two lower frequencies, 250 Hz and 50 Hz. These indicate that these four compounds do not show any slow relaxation of magnetization at zero dc field. On the other hand, the out-of-phase data for the Dy^{III} analogue are detectable, frequency-dependent, and have maxima at all of the frequencies of 5, 10. 25, 50, 250, 499, 997, and 1488 Hz, revealing that this system is a single-molecule magnet. The fitting (Figure 11) of the frequency-dependent data with the Arrhenius law ($\ln \tau = \ln \tau_0 + U_{eff}/k_BT$) provides an energy barrier (U_{eff}) of 25 cm^{-1} and a relaxation time (τ_0) of 8×10^{-8} s.

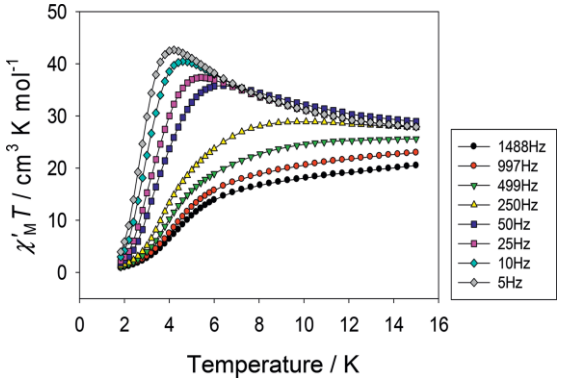

Figure 9. Plot of $\chi'_M T$ versus T of $[Ni^{II}_2Dy^{III}_2L_4(NO_3)_2(H_2O)_2]\cdot 2H_2O$ (**3A**) under zero dc field.

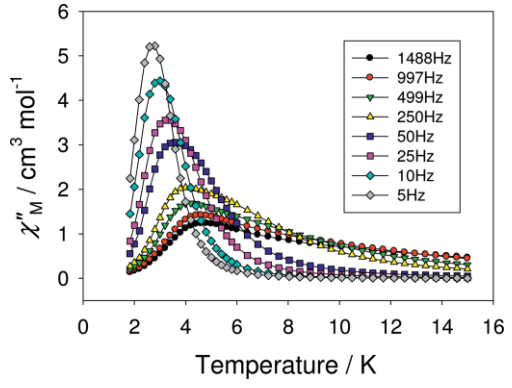

Figure 10. Plot of χ''_M versus T of $[Ni^{II}_2Dy^{III}_2L_4(NO_3)_2(H_2O)_2]\cdot 2H_2O$ (**3A**) under zero dc field.

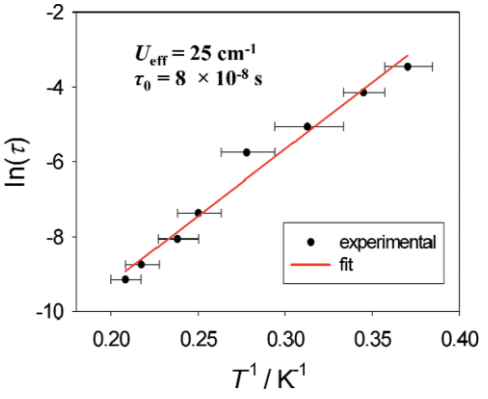

Figure 11. Arrhenius semilog plot with error bars of the relaxation time, ln(τ) versus 1/T, of compound $[Ni^{II}_2Dy^{III}_2L_4(NO_3)_2(H_2O)_2]\cdot 2H_2O$ (**3A**) from ac susceptibility measurements under zero dc field.

Comparison of the Structures/Magnetic Properties of 1–5 and 1A–5A with the Closely Related Systems

The ten compounds in this report are among the rare examples of "butterfly" $Ni^{II}_2Ln^{III}_2$ compounds.[13c,16] However, it is more relevant to compare the structures and magnetic properties of the title compounds with those of the two "butterfly" $Ni^{II}_2Tb^{III}_2$ and two "butterfly" $Ni^{II}_2Dy^{III}_2$ complexes, reported by Powell and co-workers,[16a] derived from another Schiff base ligand (H_2L^1), which is very similar to H_2L; H_2L^1 is the [1+1] condensation product of *o*-vanillin and 2-aminophenol; that is, the difference between H_2L and H_2L^1 is that the former contains an ethoxy moiety, but the latter contains a methoxy moiety at the same position. The compositions of those four compounds are $[Ni^{II}_2Ln^{III}_2L^1_4(NO_3)_2(DMF)_2]$ [Ln = Tb (**7**), Dy (**8**)] and $[Ni^{II}_2Ln^{III}_2L^1_4(NO_3)_2(MeOH)_2]\cdot 3MeOH$ [Ln = Tb (**9**), Dy (**10**)]; that is, the compositions of **7**–**10** and **1**–**5**/**1A**–**5A** are similar: $[Ni^{II}_2Ln^{III}_2L_4/L^1_4(NO_3)_2(S)_2]$ (S = DMF for **7** and **8**, MeOH for **9** and **10** and **1**–**5**, and H_2O for **1A**–**5A**). The tetrametallic core structures of the compounds **7**–**10** (Tb and Dy only) are also similar to **1**–**5** (Gd–Er) or **1A**–**5A** (Gd–Er). As already mentioned, the compounds **1A**–**5A** (where Ni^{II} is water-coordinated) are formed through SC–SC transformation of the compounds **1**–**5** (where Ni^{II} is methanol-coordinated). On the other hand, no such SC–SC transformation occurs for the compounds from H_2L^1, even for **9** and **10** (where Ni^{II} is methanol-coordinated), revealing a remarkable difference between the two related ligands.

The SMM properties of **7**–**10** have been investigated[16a] and the results are compared with those of **1A**–**5A** in Table 4. Both of the Dy^{III} compounds from H_2L^1 have been found to be SMMs, with U_{eff} values of 12.86 cm^{-1} (**8**) and 14.8 cm^{-1} (**10**). One (**7**) of the two Tb^{III} analogues from H_2L^1 is clearly not an SMM,

Table 4. Glossary of magnetic properties of the "butterfly" $[Ni^{II}_2Ln^{III}_2]$ compounds derived from H_2L and its methoxy analogue (H_2L^1).[a]

Compound	U_{eff} [cm^{-1}]	τ_0 [s]	Reference
$[Ni^{II}_2Gd^{III}_2L_4(NO_3)_2(H_2O)_2]\cdot 2H_2O$ (**1A**)	–	–	this work
$[Ni^{II}_2Tb^{III}_2L_4(NO_3)_2(H_2O)_2]\cdot 2H_2O$ (**2A**)	–	–	this work
$[Ni^{II}_2Dy^{III}_2L_4(NO_3)_2(H_2O)_2]\cdot 2H_2O$ (**3A**)	25	8×10^{-8}	this work
$[Ni^{II}_2Ho^{III}_2L_4(NO_3)_2(H_2O)_2]\cdot 2H_2O$ (**4A**)	–	–	this work
$[Ni^{II}_2Er^{III}_2L_4(NO_3)_2(H_2O)_2]\cdot 2H_2O$ (**5A**)	–	–	this work
$[Ni^{II}_2Tb^{III}_2L^1_4(NO_3)_2(DMF)_2]$ (**7**)	–	–	[16a]
$[Ni^{II}_2Dy^{III}_2L^1_4(NO_3)_2(DMF)_2]$ (**8**)	12.86	5.4×10^{-7}	[16a]
$[Ni^{II}_2Tb^{III}_2L^1_4(NO_3)_2(MeOH)_2]\cdot 3MeOH$ (**9**)	---[b]	---[b]	[16a]
$[Ni^{II}_2Dy^{III}_2L^1_4(NO_3)_2(MeOH)_2]\cdot 3MeOH$ (**10**)	14.8	1.5×10^{-6}	[16a]

[a] H_2L and H_2L^1 are the Schiff base ligands, resulting from the [1+1] condensation of, respectively, 3-ethoxysalicylaldehyde and 3-methoxysalicylaldehyde with 2-aminophenol. [b] Shows signal of slow relaxation of magnetization, but without any maximum in plots of χ_M' and χ_M'' versus T, above 1.8 K.

while the second (**9**) exhibits detectable out-of-phase susceptibilities, but the signals are weakly frequency-dependent. In the present series of **1A**–**5A** (Gd–Er), only the Dy^{III} analogue (**3A**) has been found to be a SMM, with a U_{eff} value of 25 cm^{-1}. The differences regarding the SMM properties in the similar $Ni^{II}_2Tb^{III}_2$/$Ni^{II}_2Dy^{III}_2$ compounds, derived from the two related ligands (H_2L and H_2L^1), may be summarized as follows: (i) the U_{eff} value of the $Ni^{II}_2Dy^{III}_2$, compound **3A**, derived from H_2L, is around double than that of the $Ni^{II}_2Dy^{III}_2$ compounds **8** and **10**, derived from H_2L^1; (ii) no detectable out-of-phase susceptibilities are observed for the $Ni^{II}_2Tb^{III}_2$ compound **2A**, derived from H_2L, but weak frequency-dependent out-of-phase signals are observed for the $Ni^{II}_2Tb^{III}_2$ compound **9**, derived from H_2L^1. Notably, as **3A** is a slightly better SMM than **8**/**10**, **2A** should have better detectable out-of-phase signals than **7**/**9**, which does not take place.

It is relevant to look into the structural parameters for a possible rationalization of the abovementioned differences in magnetic properties. The structural parameters of **8** (Dy^{III}) and **9** (Tb^{III}) are available, among those of **7**–**10**, and these are compared with those of **2** and **2A** (Tb^{III}) and **3** and **3A** (Dy^{III}) in Table 5 and Tables S14–S16. The Ni–N/O and Ln–N/O bond lengths and the bond angles involving the Ni^{II} center in the $Ni^{II}_2Dy^{III}_2$ compound **8** or $Ni^{II}_2Tb^{III}_2$ compound **9**, derived from H_2L^1, are very close to those of the corresponding $Ni^{II}_2Ln^{III}_2$ compounds **2**/**2A** or **3**/**3A**, derived from H_2L. However, significant differences occur in a number of bond angles involving the lanthanide(III) ion in the compounds derived from the two ligands. For example: (i) some corresponding bond angles in the DMF-coordinated $Ni^{II}_2Dy^{III}_2$ compound (**8**) of H_2L^1 and the water-coordinated $Ni^{II}_2Dy^{III}_2$ compound (**3A**) derived from H_2L differ significantly (maximum difference = 14.45°); (ii) the $Ni^{II}\cdots Dy^{III}$–O8 angle (which is a measure of the tipping of nitrate towards the Ni^{II} center) is smaller in **3A** (from H_2L, water-coordinated) than in **8** (from H_2L^1, DMF-coordinated) by 14.65°; (iii) even for the MeOH coordinated compounds of the same lanthanide, Tb^{III} (**10** and **2**), the difference in some bond angles is significant (maximum difference = 7.73°); and (iv) even for the MeOH coordinated compounds of the same lanthanide, Tb^{III} (**10** and **2**), the $Ni^{II}\cdots Tb^{III}$–O8 angle is different by 5.7°. As listed

Table 5. Comparison of some structural parameters (angles [°] and distances [Å]) around the Ln^{III} center in the Tb^{III} compounds **2A**, **2**, and **9** and the Dy^{III} compounds **3**, **3A**, and **8**.

	2A (Ni_2Tb_2)	**2** (Ni_2Tb_2)	**9** (Ni_2Tb_2)	|Δ(**2**–**9**)|	**3** (Ni_2Dy_2)	**3A** (Ni_2Dy_2)	**8** (Ni_2Dy_2)	|Δ(**3A**–**8**)|
N1–Ln1–O6	159.85(12)	159.14(16)	156.7	2.44	159.01(11)	159.33(14)	158.56	0.77
N1–Ln1–O2	68.48(11)	68.47(15)	74.6	6.13	68.51(10)	68.69(14)	67.61	1.08
O6–Ln1–O5/O5A	88.22(11)	87.51(15)	85.6	1.91	87.39(10)	87.89(13)	86.5	1.39
O1–Ln1–O8	109.53(13)	109.79(18)	103.4	6.39	109.65(12)	109.50(16)	96.63	12.87
N1–Ln1–O8	75.70(13)	76.29(17)	74.6	1.69	76.07(12)	75.52(16)	70.30	5.22
O2–Ln1–O8	77.01(11)	77.41(16)	79.8	2.39	77.38(11)	76.91(14)	85.73	8.82
O4–Ln1–O8	82.04(11)	82.37(16)	90.1	7.73	82.33(11)	82.44(14)	96.89	14.45
O6–Ln1–O8	115.03(12)	115.92(16)	121.1	5.18	115.98(11)	115.50(14)	119.30	3.8
O1–Ln1–O9	81.62(14)	82.39(19)	85.3	2.91	82.01(14)	81.24(17)	81.04	0.2
N1–Ln1–O9	108.96(14)	109.93(18)	115.8	5.87	109.86(13)	108.87(17)	113.43	4.56
O2–Ln1–O9	124.81(12)	124.96(18)	122.1	2.86	124.85(12)	125.10(15)	127.37	2.27
O4–Ln1–O9	84.21(13)	84.13(18)	80.6	3.53	83.87(13)	84.67(15)	84.92	0.25
O6–Ln1–O9	70.70(13)	71.22(18)	71.8	0.58	71.10(12)	70.70(16)	68.91	1.79
O8–Ln1–O5/O5A	150.38(12)	149.97(17)	150.8	0.83	150.33(11)	150.42(14)	154.15	3.73
O9–Ln1–O5/O5A	157.77(13)	157.93(18)	157.3	0.63	157.65(12)	157.38(16)	153.75	3.63
Ni1···Ln1–O8	73.9	74.1	79.8	5.7	74.11	73.95	88.6	14.65
Ni1···Ln1–O9	103.09	102.64	98.7	3.94	102.6	103.35	105.2	1.85
Ln1···Ni1–O7	89.02	86.88	85.1	1.78	87.04	89.06	89.5	0.44
$d(NO_3)$[a]	0.026	0.019	0.103	0.084	0.019	0.03	0.130	0.1
$d(O_4)$[b]	0.293	0.291	0.298	0.005	0.289	0.293	0.298	0.005
δ[c]	0.4	0.4	2.02	1.62	0.3	0.4	7.15	6.75

[a] Average deviation [Å] of the four O/N atoms from the least-squares NO_3 "square" plane. [b] Average deviation [Å] of the four O atoms from the least-squares O_4 "square" plane. [c] Dihedral angle [°] between the least-squares NO_3 and O_4 "square" planes.

in Table 3, the "most ideal" coordination geometry for **1**–**5**/**1A**–**5A**, as well as of **8** and **9**, is triangular-dodecahedron (TDD). However, the coordination geometry is better perceived as distorted square-antiprism (SAPR; see Figure S25 for a representative illustration; notably, the deviations for SAPR and TDD are not very different); considering this geometry, another significant difference in the structures of the compounds from the two ligands may be understood, and that is that the dihedral angle between the two square planes is different by 1.62° for the Tb^{III} case and by 6.75° for the Dy^{III} case. All of these differences in the structural parameters impose a subtle effect to induce a significant difference in the magnetic properties of the similar "butterfly" $Ni^{II}_2Tb^{III}_2$/$Ni^{II}_2Dy^{III}_2$ compounds (of similar composition) derived from the two related ligands.

Conclusion

The ten "butterfly" compounds $Ni^{II}_2Ln^{III}_2$ (Ln = Gd, Tb, Dy, Ho, Er), compounds **1**–**5** and **1A**–**5A**, are the second set of examples (next to the $Zn^{II}_2Dy^{III}_2$/$Co^{II}_2Dy^{III}_2$/$Mn^{II}_2Dy^{III}_2$ compounds reported very recently,[19] during the progress of the present investigation) of 3d–4f systems derived from a Schiff base ligand, obtained on [1+1] condensation of 3-ethoxysalicylaldehyde and an amino alcohol or aminophenol (the latter component in this study is 2-aminophenol; the ligand is H_2L).

Interestingly, single-crystal to single-crystal transformations from **1**–**5** to **1A**–**5A**, where all ten compounds are isomorphous, are among only a few examples in which a ligand (solvent) in the inner coordination sphere is substituted by another ligand (solvent).

The magnetic properties of $Ni^{II}_2Ln^{III}_2$ compounds **1A**–**5A** reveal overall ferromagnetic interaction in all of these five compounds. Simulation of the data of the Gd^{III} analogues indicates that both the Ni^{II}···Ni^{II} and the Ni^{II}···Gd^{III} interactions are ferromagnetic.

Comparison of the $Ni^{II}_2Ln^{III}_2$ compounds **1**–**5** and **1A**–**5A**, derived from 3-ethoxysalicylaldehyde–2-aminophenol ligand H_2L, with four $Ni^{II}_2Tb^{III}_2$/$Ni^{II}_2Dy^{III}_2$ compounds derived from the 3-methoxysalicylaldehyde–2-aminophenol ligand H_2L^1, reveal that similar "butterfly" compounds are stabilized in the environment of both ligands. However, comparison of the Tb^{III}/Dy^{III} analogues from the two ligands reveals some remarkable differences in a number of bond angles involving the lanthanide(III) center, which are reflected in the SMM properties: (i) the U_{eff} value of the Dy^{III} analogue from H_2L is almost two times greater than that of the Dy^{III} analogue from H_2L^1; and (ii) the Tb^{III} analogue from H_2L is clearly not a SMM, whereas one Tb^{III} analogue from H_2L^1 shows slow relaxation of magnetization. A difference from a structural point of view is that the methanol-coordinated (coordinated to Ni^{II}) $Ni^{II}_2Ln^{III}_2$ "butterflies" from H_2L exhibit SC–SC transformation, whereas the equivalent compounds from H_2L^1 do not show such a phenomenon. All in all, some remarkable differences have been observed in the 3d–4f clusters derived from two related ligands. As many 3d–4f clusters are known to be derived from 3-methoxysalicylaldehyde–amino alcohol/aminophenol Schiff base ligands, we hope that 3d–4f systems from 3-ethoxysalicylaldehyde–amino alcohol/aminophenol Schiff base ligands will be extensively addressed in the future. In fact, a number of such works are under progress in our laboratory.

Experimental Section

Materials and Physical Measurements: All of the reagents and solvents were purchased from commercial sources and were used as received. Elemental (C, H, and N) analyses were performed with a Perkin–Elmer 2400 II analyzer. IR spectra were recorded in the region 400–4000 cm^{-1} with a Bruker Optics Alpha–T spectrophotometer, with samples as KBr disks. The magnetic measurements were carried out with a SQUID-VSM (Quantum Design) instrument at the University of Calcutta (the *M*-H data) and a SQUID magnetometer (MPMS, Quantum Design) at the University of Florida (other data).

Synthesis of H_2L: A solution of 2-aminophenol (0.546 g, 5 mmol) in methanol (10 mL) was added dropwise to a methanol solution (50 mL) of 3-ethoxysalicylaldehyde (0.831 g, 5 mmol) while being warmed. The reaction mixture was refluxed for 3 h. Then, the resulting solution was concentrated to 25 mL and was filtered to remove the very fine suspended particles. The filtrate was allowed to slowly evaporate. The deposited red crystalline compound, H_2L, was collected by filtration and was washed with cold methanol.

Syntheses of $[Ni^{II}_2Ln^{III}_2L_4(NO_3)_2(MeOH)_2]$ (1, Ln = Gd; 2, Ln = Tb; 3, Ln = Dy; 4, Ln = Ho; 5, Ln = Er)

The five compounds were prepared following a general procedure, as follows: A methanol solution (5 mL) of the corresponding hydrated Ln $(NO_3)_3$ (0.1 mmol) and a methanol solution (5 mL) of Et_3N (0.04 g, 0.4 mmol) were successively added dropwise to a methanol solution (25 mL) of H_2L (0.052 g, 0.2 mmol) whilst stirring. After stirring for 30 min, a methanol solution (5 mL) of $Ni(NO_3)_2{\cdot}6H_2O$ (0.029 g, 0.1 mmol) was added whilst stirring. Then the mixture was filtered to remove any suspended particles and the filtrate was kept at ambient temperature to slowly evaporate. After one–two days, the deposited green crystalline compounds, containing diffraction quality crystals, were collected by filtration, washed with cold methanol, and dried in vacuo.

Data for 1: $C_{62}H_{60}N_6O_{20}Ni_2Gd_2$ (1641.09 g/mol). Selected FTIR data (KBr): $\tilde{\nu}$(C=N) = 1604 (vs); $\tilde{\nu}(NO_3)$ = 1386 (vs), 1292 (s); $\tilde{\nu}$(MeOH) = 3356 (m).

Data for 2: $C_{62}H_{60}N_6O_{20}Ni_2Tb_2$ (1644.43 g/mol). Selected FTIR data (KBr): $\tilde{\nu}$(C=N) = 1604 (vs); $\tilde{\nu}(NO_3)$ = 1386 (vs), 1292 (s); $\tilde{\nu}$(MeOH) = 3357 (m).

Data for 3: $C_{62}H_{60}N_6O_{20}Ni_2Dy_2$ (1651.59 g/mol). Selected FTIR data (KBr): $\tilde{\nu}$(C=N) = 1605 (vs); $\tilde{\nu}(NO_3)$ = 1388 (vs), 1292 (s); $\tilde{\nu}$(MeOH) = 3356 (m).

Data for 4: $C_{62}H_{60}N_6O_{20}Ni_2Ho_2$ (1656.44 g/mol). Selected FTIR data (KBr): $\tilde{\nu}$(C=N) = 1605 (vs); $\tilde{\nu}(NO_3)$ = 1385 (vs), 1292 (s); $\tilde{\nu}$(MeOH) = 3358 (m).

Data for 5: $C_{62}H_{60}N_6O_{20}Ni_2Er_2$ (1661.11 g/mol). Selected FTIR data (KBr): $\tilde{\nu}$(C=N) = 1606 (vs); $\tilde{\nu}(NO_3)$ = 1386 (vs), 1292 (s); $\tilde{\nu}$(MeOH) = 3358 (m).

Syntheses of $[Ni^{II}_2Ln^{III}_2L_4(NO_3)_2(H_2O)_2]{\cdot}2H_2O$ (1A, Ln = Gd; 2A, Ln = Tb; 3A, Ln = Dy; 4A, Ln = Ho; 5A, Ln = Er)

Exposing the crystalline compounds **1**–**5** to the open atmosphere for one day resulted in the formation of compounds **1A**–**5A**, which are also single crystals; their colors are the same as those of **1**–**5**.

Data for 1A: Yield: 0.068 g (82 %). $C_{60}H_{60}Gd_2N_6Ni_2O_{22}$ (1649.06 g/mol): calcd. C 43.70, H 3.67, N 5.1; found C 43.73, H 3.66, N 5.11. Selected FTIR data (KBr): $\tilde{\nu}$(C=N) = 1604 (vs); $\tilde{\nu}(NO_3)$ = 1385 (vs), 1298 (s); $\tilde{\nu}(H_2O)$ = 3418 (w).

Data for 2A: Yield: 0.070 g (85 %). $C_{60}H_{60}N_6Ni_2O_{22}Tb_2$ (1652.41 g/mol): calcd. C 43.61, H 3.66, N 5.09; found C 43.40, H 3.71, N 5.23. Selected FTIR data (KBr): $\tilde{\nu}$(C=N) = 1604 (vs); $\tilde{\nu}(NO_3)$ = 1386 (vs), 1293 (s); $\tilde{\nu}(H_2O)$ = 3425 (w).

Data for 3A: Yield: 0.075 g (90 %). $C_{60}H_{60}Dy_2N_6Ni_2O_{22}$ (1659.56 g/mol): calcd. C 43.43, H 3.64, N 5.06; found C 43.24, H 3.51, N 5.21. Selected FTIR data (KBr): $\tilde{\nu}$(C=N) = 1604 (vs); $\tilde{\nu}(NO_3)$ = 1388 (vs), 1293 (s); $\tilde{\nu}(H_2O)$ = 3426 (w).

Data for 4A: Yield: 0.072 g (87 %). $C_{60}H_{60}Ho_2N_6Ni_2O_{22}$ (1664.42 g/mol): calcd. C 43.3, H 3.63, N 5.05; found C 43.52, H 3.52, N 5.12. Selected FTIR data (KBr): $\tilde{\nu}$(C=N) = 1605 (vs); $\tilde{\nu}(NO_3)$ = 1388 (vs), 1297 (s); $\tilde{\nu}(H_2O)$ = 3427 (w).

Data for 5A: Yield: 0.071 g (85 %). $C_{60}H_{60}Er_2N_6Ni_2O_{22}$ (1669.08 g/mol): calcd. C 43.18, H 3.62, N 5.04; found C 43.35, H 3.67, N 5.19. Selected FTIR data (KBr): $\tilde{\nu}$(C=N) = 1605 (vs); $\tilde{\nu}(NO_3)$ = 1386 (vs), 1298 (s); $\tilde{\nu}(H_2O)$ = 3426 (w).

Crystal Structure Determination of 1–5 and 1A–5A: The crystallographic data of the compounds **1**–**5** and **1A**–**5A** are summarized in Tables S2 and 1, respectively. Diffraction data of the ten crystals were collected at 296 K with a Bruker-APEX II SMART CCD diffractometer using graphite-monochromated Mo-K_α radiation (λ = 0.71073 Å). As the crystals of all compounds **1**–**5** change to those of **1A**–**5A** when the crystal are exposed to air, data of **1**–**5** were collected on mounting a crystal dipped in its mother liquor in a capillary. The packages SAINT[28a] and SADABS[28b] were used for data processing and absorption correction. The structures were solved by direct and Fourier methods and were refined by full-matrix least-squares based on F^2 using the SHELXS-97[28c] and SHELXL-2014/7[28d] packages. Hydrogen atoms of two solvated water molecules in **1A**–**5A** could not be located from difference Fourier maps and were therefore not considered in the refinement. All other hydrogen atoms in **1**–**5** and **1A**–**5A** were inserted at calculated positions with isotropic thermal parameters and were refined. All of the non-hydrogen atoms were refined anisotropically, while all of the hydrogen atoms were refined isotropically. The final refinement converged to R_1 [$I > 2\sigma(I)$] values of 0.0403, 0.0460, 0.0347, 0.0410, and 0.0449 for **1**–**5**, respectively, and 0.0408, 0.0364, 0.0404, 0.0333, and 0.0409 for **1A**–**5A**, respectively.

CCDC 1815023 (for **1**), 1815024 (for **2**), 1815025 (for **3**), 1815026 (for **4**), 1815027 (for **5**), 1815029 (for **1A**), 1815030 (for **2A**), 1815031 (for **3A**), 1815032 (for **4A**), and 1815033 (for **5A**) contain the supplementary crystallographic data for this paper. These data can be obtained free of charge from The Cambridge Crystallographic Data Center.

Supporting Information: (see footnote on the second page of this article): Figures S1–S25 and Tables S1–S16.

Acknowledgments

Financial support for this work has been received from the Government of India through the University Grants Commission (contingency from CAS-V project to S. Mohanta), the Department of Science and Technology (INSPIRE Fellowship to S. Mandal), and the Council of Scientific and Industrial Research (fellowship to S. G.). Crystallography was performed at the DST-FIST-funded Single Crystal Diffractometer Facility at the Department of Chemistry, University of Calcutta. The Center for Research in Nanoscience and Nanotechnology (CRNN), University of Calcutta, is acknowledged for magnetic data (*M-H*; Figure 7 and Figures S13–S16). G. C. thanks the USA National Science foundation for support (CHE-1565664).

Keywords: Single-molecule magnets · Ferromagnetic interactions · SC–SC transformations · Lanthanides · Butterfly complexes

[1] R. Sessoli, D. Gatteschi, A. Caneschi, M. A. Novak, *Nature* **1993**, *365*, 141.
[2] a) C. Benelli, D. Gatteschi (Eds.), *Introduction to Molecular Magnetism: From Transition Metals to Lanthanides*, Wiley-VCH, Weinheim, **2015**; b) W. Linert, M. Verdaguer Eds (Eds.), *Molecular Magnets Recent Highlights*, Springer, New York, **2012**; c) R. E. P. Winpenny, G. Aromí, *Single-Molecule Magnets and Related Phenomena*, Springer-Verlag, Berlin, **2006**; d) D. Gatteschi, R. Sessoli, J. Villain, *J. Molecular Nanomagnets*, Oxford University Press, Oxford, **2006**; e) D. Gatteschi, *Adv. Mater.* **1994**, *6*, 635; f) Molecular spintronics and quantum computing: J. Lehmann, A. Gaita-Ariño, E. Coronadoc, D. Loss, *J. Mater. Chem.* **2009**, *19*, 1670; g) L. Bogani, W. Wernsdorfer, *Nat. Mater.* **2008**, *7*, 179; h) Y.-Z. Zheng, G.-J. Zhou, Z. Zheng, R. E. P. Winpenny, *Chem. Soc. Rev.* **2014**, *43*, 1462.
[3] a) S. M. J. Aubin, M. W. Wemple, D. M. Adams, H.-L. Tsai, G. Christou, D. N. Hendrickson, *J. Am. Chem. Soc.* **1996**, *118*, 7746; b) S. M. J. Aubin, N. R. Dilley, M. W. Wemple, M. B. Maple, G. Christou, D. N. Hendrickson, *J. Am. Chem. Soc.* **1998**, *120*, 839; c) H. Andres, F. Basler, H.-U. Güdel, G. Aromí, G. Christou, H. Büttner, B. Rufflé, *J. Am. Chem. Soc.* **2000**, *122*, 12469; d) T. C. Stamatatos, G. Christou, *Inorg. Chem.* **2009**, *48*, 3308; e) S. Mukherjee, K. A. Abboud, W. Wernsdorfer, G. Christou, *Inorg. Chem.* **2013**, *52*, 873.
[4] a) G. Aromí, E. K. Brechin, *Struct. Bonding (Berlin)* **2006**, *122*, 1; b) M. Murrie, *Chem. Soc. Rev.* **2010**, *39*, 1986.
[5] N. Ishikawa, M. Sugita, T. Ishikawa, S. Koshihara, Y. Kaizu, *J. Am. Chem. Soc.* **2003**, *125*, 8694.
[6] a) L. Sorace, C. Benelli, D. Gatteschi, *Chem. Soc. Rev.* **2011**, *40*, 3092; b) D. N. Woodruff, R. E. P. Winpenny, R. A. Layfield, *Chem. Rev.* **2013**, *113*, 5110; c) R. Sessoli, A. K. Powell, *Coord. Chem. Rev.* **2009**, *253*, 2328.
[7] a) C. A. P. Goodwin, F. Ortu, D. Reta, N. F. Chilton, D. P. Mills, *Nature* **2017**, *548*, 439; b) S. K. Gupta, T. Rajeshkumar, G. Rajaraman, R. Murugavel, *Chem. Sci.* **2016**, *7*, 5181; c) J. Liu, Y.-C. Chen, J.-L. Liu, V. Vieru, L. Ungur, J.-H. Jia, L. F. Chibotaru, Y. Lan, W. Wernsdorfer, S. Gao, X.-M. Chen, M.-L. Tong, *J. Am. Chem. Soc.* **2016**, *138*, 5441; d) Y.-S. Ding, N. F. Chilton, R. E. P. Winpenny, Y.-Z. Zheng, *Angew. Chem. Int. Ed.* **2016**, *55*, 16071; *Angew. Chem.* **2016**, *128*, 16305; e) Y.-C. Chen, J.-L. Liu, L. Ungur, J. Liu, Q.-W. Li, L.-F. Wang, Z.-P. Ni, L. F. Chibotaru, X.-M. Chen, M.-L. Tong, *J. Am. Chem. Soc.* **2016**, *138*, 2829; f) J. J. L. Roy, L. Ungur, I. Korobkov, L. F. Chibotaru, M. Murugesu, *J. Am. Chem. Soc.* **2014**, *136*, 8003; g) A. Upadhyay, K. R. Vignesh, C. Das, S. K. Singh, G. Rajaraman, M. Shanmugam, *Inorg. Chem.* **2017**, *56*, 14260.
[8] a) F. Habib, P.-H. Lin, J. Long, I. Korobkov, W. Wernsdorfer, M. Murugesu, *J. Am. Chem. Soc.* **2011**, *133*, 8830; b) I. J. Hewitt, J. Tang, N. T. Madhu, C. E. Anson, Y. Lan, J. Luzon, M. Etienne, R. Sessoli, A. K. Powell, *Angew. Chem. Int. Ed.* **2010**, *49*, 6352; *Angew. Chem.* **2010**, *122*, 6496; c) S. Das, A. Dey, S. Biswas, E. Colacio, V. Chandrasekhar, *Inorg. Chem.* **2014**, *53*, 3417; d) V. Chandrasekhar, P. Bag, E. Colacio, *Inorg. Chem.* **2013**, *52*, 4562.
[9] a) C. Das, S. Vaidya, T. Gupta, J. M. Frost, M. Righi, E. K. Brechin, M. Affronte, G. Rajaraman, M. Shanmugam, *Chem. Eur. J.* **2015**, *21*, 15639; b) Y.-Z. Zheng, Y. Lan, C. E. Anson, A. K. Powell, *Inorg. Chem.* **2008**, *47*, 10813; c) H.-H. Zou, R. Wang, Z.-L. Chen, D.-C. Liu, F.-P. Liang, *Dalton Trans.* **2014**, *43*, 2581; d) A. K. Jami, V. Baskar, E. C. Sanudo, *Inorg. Chem.* **2013**, *52*, 2432; e) S. Shen, S. Xue, S.-Y. Lin, L. Zhao, J. A. Tang, *Dalton Trans.* **2013**, *42*, 10413; f) H. Ke, G.-F. Xu, L. Zhao, J. Tang, X.-Y. Zhang, H.-J. Zhang, *Chem. Eur. J.* **2009**, *15*, 10335; g) H. Ke, L. Zhao, G.-F. Xu, Y.-N. Guo, J. Tang, X.-Y. Zhang, H.-J. Zhang, *Dalton Trans.* **2009**, 10609.
[10] a) H. L. C. Feltham, R. Clérac, L. Ungur, L. F. Chibotaru, A. K. Powell, S. Brooker, *Inorg. Chem.* **2013**, *52*, 3236; b) H. L. C. Feltham, R. Clérac, A. K. Powell, S. Brooker, *Inorg. Chem.* **2011**, *50*, 4232; c) V. Mereacre, Y. Lan, R.

Clérac, A. M. Ako, W. Wernsdorfer, G. Buth, C. F. Anson, A. K. Powell, *Inorg. Chem.* **2011**, *50*, 12001; d) H.-R. Wen, P.-P. Dong, S.-J. Liu, J.-S. Liao, F.-Y. Liang, C.-M. Liu, *Dalton Trans.* **2017**, *46*, 1153; e) K.-Q. Hu, X. Jiang, S.-Q. Wu, C.-M. Liu, A.-L. Cui, H.-Z. Kou, *Inorg. Chem.* **2015**, *54*, 1206; f) J. Wu, L. Zhao, L. Zhang, X.-L. Li, M. Guo, A. K. Powell, J. Tang, *Angew. Chem. Int. Ed.* **2016**, *55*, 15574; *Angew. Chem.* **2016**, *128*, 15803; g) J. Wu, X.-L. Li, M. Guo, L. Zhao, Y.-Q. Zhang, J. Tang, *Chem. Commun.* **2018**, *54*, 1065.

[11] a) S. K. Langley, C. Le, L. Ungur, B. Moubaraki, B. F. Abrahams, L. F. Chibotaru, K. S. Murray, *Inorg. Chem.* **2015**, *54*, 3631; b) A. V. Funes, L. Carrella, Y. Rechkemmer, J. van Slageren, E. Rentschler, P. Alborés, *Dalton Trans.* **2017**, *46*, 3400; c) K. R. Vignesh, S. K. Langley, K. S. Murray, G. Rajaraman, *Inorg. Chem.* **2017**, *56*, 2518; d) A. V. Funes, L. Carrella, E. Rentschler, P. Alborés, *Dalton Trans.* **2014**, *43*, 2361.

[12] S. K. Langley, D. P. Wielechowski, N. F. Chilton, B. Moubaraki, K. S. Murray, *Inorg. Chem.* **2015**, *54*, 10497.

[13] a) C. Papatriantafyllopoulou, K. A. Abboud, G. Christou, *Inorg. Chem.* **2011**, *50*, 8959; b) A. S. R. Chesman, D. R. Turner, K. J. Berry, N. F. Chilton, B. Moubaraki, K. S. Murray, G. B. Deacon, S. R. Batten, *Dalton Trans.* **2012**, *41*, 11402; c) E. M. Pineda, N. F. Chilton, F. Tuna, R. E. P. Winpenny, E. J. L. McInnes, *Inorg. Chem.* **2015**, *54*, 5930; d) M. N. Akhtar, Y. Lan, V. Mereacre, R. Clérac, C. E. Anson, A. K. Powell, *Polyhedron* **2009**, *28*, 1698.

[14] a) M. Murugesu, A. Mishra, W. Wernsdorfer, K. A. Abboud, G. Christou, *Polyhedron* **2006**, *25*, 613; b) A. Baniodeh, Y. Lan, G. Novitchi, V. Mereacre, A. Sukhanov, M. Ferbinteanu, V. Voronkova, C. E. Anson, A. K. Powell, *Dalton Trans.* **2013**, *42*, 8926.

[15] Y. Peng, V. Mereacre, C. E. Ansona, A. K. Powell, *Dalton Trans.* **2017**, *46*, 5337.

[16] a) K. C. Mondal, G. E. Kostakis, Y. Lan, W. Wernsdorfer, C. E. Anson, A. K. Powell, *Inorg. Chem.* **2011**, *50*, 11604; b) K. Griffiths, C. W. D. Gallop, A. Abdul-Sada, A. Vargas, O. Navarro, G. E. Kostakis, *Chem. Eur. J.* **2015**, *21*, 6358; c) H.-H. Zou, L.-B. Sheng, F.-P. Liang, Z.-L. Chena, Y.-Q. Zhang, *Dalton Trans.* **2015**, *44*, 18544.

[17] a) P. Bag, A. Chakraborty, G. Rogez, V. Chandrasekhar, *Inorg. Chem.* **2014**, *53*, 6524; b) V. Chandrasekhar, P. Bag, M. Speldrich, J. v. Leusen, P. Kögerler, *Inorg. Chem.* **2013**, *52*, 5035; c) J. Goura, J. Brambleby, P. Goddard, V. Chandrasekhar, *Chem. Eur. J.* **2015**, *21*, 4926; d) N. Ahmed, C. Das, S. Vaidya, S. K. Langley, K. S. Murray, M. Shanmugam, *Chem. Eur. J.* **2014**, *20*, 14235; e) H. Ke, L. Zhao, Y. Guo, J. Tang, *Inorg. Chem.* **2012**, *51*, 2699; f) I. A. Kühne, G. E. Kostakis, C. E. Anson, A. K. Powell, *Inorg. Chem.* **2016**, *55*, 4072; g) H. Ke, L. Zhao, Y. Guoa, J. Tang, *Dalton Trans.* **2012**, *41*, 2314.

[18] a) V. Chandrasekhar, A. Dey, S. Das, S. Kundu, *CrystEngComm* **2014**, *16*, 1304; b) G. Wu, I. J. Hewitt, S. Mameri, Y. Lan, R. Clérac, C. E. Anson, S. Qiu, A. K. Powell, *Inorg. Chem.* **2007**, *46*, 7229; c) I. Nemec, M. Machata, R. Herchel, R. Boča, Z. Trávníček, *Dalton Trans.* **2012**, *41*, 14603.

[19] J. Li, R.-M. Wei, T.-C. Pu, F. Cao, L. Yang, Y. Han, Y.-Q. Zhang, J.-L. Zuo, Y. Song, *Inorg. Chem. Front.* **2017**, *4*, 114.

[20] a) A. Biswas, L. Mandal, S. Mondal, C. R. Lucas, S. Mohanta, *CrystEngComm* **2013**, *15*, 5888; b) P. Chakraborty, A. Jana, S. Mohanta, *Polyhedron* **2014**, *77*, 39; c) S. Majumder, R. Koner, P. Lemoine, M. Nayak, M. Ghosh, S. Hazra, C. R. Lucas, S. Mohanta, *Eur. J. Inorg. Chem.* **2009**, 3447; d) A. Biswas, M. Ghosh, P. Lemoine, S. Sarkar, S. Hazra, S. Mohanta, *Eur. J. Inorg. Chem.* **2010**, 3125; e) S. Bhattacharya, A. Jana, S. Mohanta, *Polyhedron* **2013**, *62*, 234.

[21] a) J. Cirera, E. Ruiz, S. Alvarez, *Chem. Eur. J.* **2006**, *12*, 3162; b) M. Pinsky, D. Avnir, *Inorg. Chem.* **1998**, *37*, 5575.

[22] a) S. M. Neville, G. J. Halder, K. W. Chapman, M. B. Duriska, P. D. Southon, J. D. Cashion, J.-F. Létard, B. Moubaraki, K. S. Murray, C. J. Kepert, *J. Am. Chem. Soc.* **2008**, *130*, 2869; b) A. Aijaz, P. Lama, P. K. Bharadwaj, *Inorg. Chem.* **2010**, *49*, 5883; c) R. Dey, R. Haldar, T. K. Maji, D. Ghoshal, *Cryst. Growth Des.* **2011**, *11*, 3905.

[23] a) Y.-C. He, J. Yang, Y.-Y. Liu, J.-F. Malnorg, *Inorg. Chem.* **2014**, *53*, 7527; b) A. Husain, M. Ellwart, S. A. Bourne, L. Öhrström, C. L. Oliver, *Cryst. Growth Des.* **2013**, *13*, 1526.

[24] a) P. B. Chatterjee, A. Audhya, S. Bhattacharya, S. M. T. Abtab, K. Bhattacharya, M. Chaudhury, *J. Am. Chem. Soc.* **2010**, *132*, 15842; b) G.-L. Li, W.-D. Yin, G.-Z. Liu, L.-F. Ma, L.-L. Huang, L. Li, L.-Y. Wang, *Inorg. Chem. Commun.* **2014**, *43*, 165.

[25] a) D. Sarma, S. Natarajan, *Cryst. Growth Des.* **2011**, *11*, 5415; b) H.-Y. Ren, R.-X. Yao, X.-M. Zhang, *Inorg. Chem.* **2015**, *54*, 6312; c) S. M. Mobin, A. K. Srivastava, P. Mathur, G. K. Lahiri, *Inorg. Chem.* **2009**, *48*, 4652.

[26] a) S. Supriya, S. K. Das, *J. Am. Chem. Soc.* **2007**, *129*, 3464; b) M. C. Das, P. K. Bharadwaj, *J. Am. Chem. Soc.* **2009**, *131*, 10942; c) R. Singh, J. Mrozinski, P. K. Bharadwaj, *Cryst. Growth Des.* **2014**, *14*, 3623; d) J. Yao, J.-M. Chen, Y.-B. Xu, T.-B. Lu, *Cryst. Growth Des.* **2014**, *14*, 5019; e) M. J. Manos, E. J. Kyprianidou, G. S. Papaefstathiou, A. J. Tasiopoulos, *Inorg. Chem.* **2012**, *51*, 6308; f) E. J. Kyprianidou, T. Lazarides, S. Kaziannis, C. Kosmidis, G. Itskos, M. J. Manos, A. J. Tasiopoulos, *J. Mater. Chem. A* **2014**, *2*, 5258.

[27] N. F. Chilton, R. P. Anderson, L. D. Turner, A. Soncini, K. S. Murray, *J. Comput. Chem.* **2013**, *34*, 1164.

[28] a) *Bruker-Nonius*, *APEX-II*, *SAINT-Plus* and *TWINABS*, Bruker-Nonius AXS Inc. Madison, Wisconsin, USA, **2004**; b) G. M. Sheldrick, *SAINT* (Version 6.02), *SADABS* (Version 2.03), Bruker AXS Inc. Madison, Wisconsin, USA, **2002**; c) G. M. Sheldrick, *SHELXS-97*, *Crystal Structure Solution Program*, University of Göttingen, Germany, **2008**; d) G. M. Sheldrick, *SHELXL-2014/7*, *Crystal Structure Refinement Program*, University of Göttingen, Germany, **2014**; e) Spek, A. L. *PLATON*, *A Multipurpose Crystallographic Tool*, Utrecht University, The Netherlands, **2008**.

Received: March 20, 2018

